# Development of an optimised LSO/LuYAP phoswich detector head for the ClearPET camera

J.-B. Mosset, O. Devroede, M. Krieguer, M. Rey, J.-M. Vieira, J. H. Jung, C. Kuntner, M. Streun, K. Ziemons, E. Auffray, P. Sempere-Roldan, P. Lecoq, P. Bruyndonckx, J.-F. Loude, S. Tavernier, C. Morel

***Abstract*— The paper describes the LSO/LuYAP phoswich detector head developed for the ClearPET small animal PET scanner demonstrator that is under construction within the Crystal Clear Collaboration. The detector head consists of a dual layer of 8 x 8 LSO and LuYAP crystal arrays coupled to a multi-channel photomultiplier tube (Hamamatsu R7600-M64). Equalisation of the LSO/LuYAP light collection is obtained through partial attenuation of the LSO scintillation light using a thin aluminium deposit of 20-35 nm on LSO and appropriate temperature regulation of the phoswich head between 30 to 60° C. At 511 keV, typical FWHM energy resolutions of the pixels of a phoswich head amounts to $(28 \pm 2)\%$ for LSO and $(25 \pm 2)\%$ for LuYAP. The LSO versus LuYAP crystal identification efficiency is better than 98%. Six detector modules have been mounted on a rotating gantry. Axial and tangential spatial resolutions were measured up to 4 cm from the scanner axis and compared to Monte Carlo simulations using GATE. FWHM spatial resolution ranges from 1.3 mm on axis to 2.6 mm at 4 cm from the axis.**

***Index Terms*— Positron emission tomography, phoswich detector, depth-of-interaction, small animal PET scanner.**

## I. Introduction

POSITRON Emission Tomography (PET) applied to small animal imaging is a potentially important tool in developing new drugs and imaging gene expression. Human scanners, which have a spatial resolution of the order of 3-4 mm, do not allow to resolve and quantify radiotracer concentration within sub-organ structures in small animals. Consequently, biomedical research groups and pharmaceutical companies are interested in running dedicated high-resolution small animal PET scanners. We describe the development and the performance measurements of an optimised LSO/LuYAP phoswich detector head for the ClearPET high resolution small animal PET scanner demonstrator that is under construction in Lausanne within the CERN Crystal Clear Collaboration (CCC) [1].

J.-B. Mosset, M. Rey, J.-M. Vieira, J.-F. Loude and C. Morel are with the Swiss Federal Institute of Technology (EPFL), 1015 Lausanne, Switzerland.

O. Devroede, M. Krieguer, P. Bruyndonckx and S. Tavernier are with the Vrije Universiteit Brussel, 1050 Brussels, Belgium.

J. H. Jung is with the Sungkyunkwan University School of Medicine, Seoul 135-710, Korea.

M. Streun and K. Ziemons are with the Forschungszentrum Jülich, 52425 Jülich, Germany.

C. Kuntner, E. Auffray, P. Sempere-Roldan and P. Lecoq are with CERN, 1211 Geneva 23, Switzerland.

All authors are members of the Crystal Clear Collaboration.

This work was supported by the Swiss National Science Foundation under grants nos. 2153-063870 and 205320-100472.

With small diameter tomographs, the uncertainty on the depth-of-interaction (DOI) of the impinging photon in the scintillating crystal results in parallax errors that degrade image resolution when getting away from the axis of the tomograph. To overcome this problem, it is possible to limit the thickness of the detector. However, signal-to-noise ratio in the voxels of the image strongly depends of the statistics acquired by the tomograph. Therefore, it is quite important to improve both spatial resolution and sensitivity in order to optimise quantitation. Thus, many approaches are currently being explored to measure DOI. This would allow to use thicker detectors and consequently to improve their sensitivity without degrading spatial resolution. The phosphor sandwich or *phoswich* approach consists in identifying the crystal of interaction by using pulse shape discrimination of signals generated by a sandwich of different scintillating materials [2], [3]. In order to achieve high sensitivity and high spatial resolution, the ClearPET scanner prototypes implement a dual layer phoswich design of LSO [4] and LuYAP [5], [6] scintillating pixels.

## II. Material and Method

### A. Design of the detector head

The LSO/LuYAP phoswich detector head uses a Hamamatsu R7600-M64 multi-channel photomultiplier tube (MCPMT). The MCPMT have a sensitive area of 18.1 x 18.1 $mm^2$ read out by a matrix of 8 x 8 individual anodes. The MCPMT channels are coupled one by one to 64 LuYAP [7] crystal elements which compose the first layer of the phoswich assembly. The second layer is composed of 64 LSO crystal elements aligned in columns above the LuYAP crystals. Every crystal is mechanically polished on all sides and measures 2.0 x 2.0 x 8.0 $mm^3$. The crystal pillars are held in a matrix of Tyvek™. The use of Tyvek maximizes the light collection and provides an optical isolation between adjacent crystal pillars. The pitch of the crystal pillars is 2.3 mm and matches the pitch of the MCPMT channels. A light attenuating metallic mask [8] is glued on the MCPMT to correct for variation in quantum efficiency of the 64 channels. Optical coupling of the LuYAP crystals to the MCPMT is obtained by gluing the crystals on the photocathode window through the metallic mask with a high viscosity glue (3145 RTV, DOW CORNING) that does not creep between the Tyvek and the crystals. Figure 1 shows a picture of a detector head at different fabrication stages and Figure 2 the phoswich detector modules in final form.

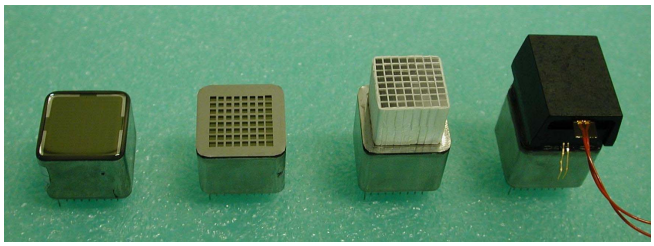

Fig. 1. Detector heads at different fabrication stages : from left to right, bare MCPMT, light attenuating mask glued on the MCPMT, scintillating crystals in a Tyvek matrix glued on the MCPMT through the mask, and MCPMT covered with a light tight cap enclosing the crystal array.

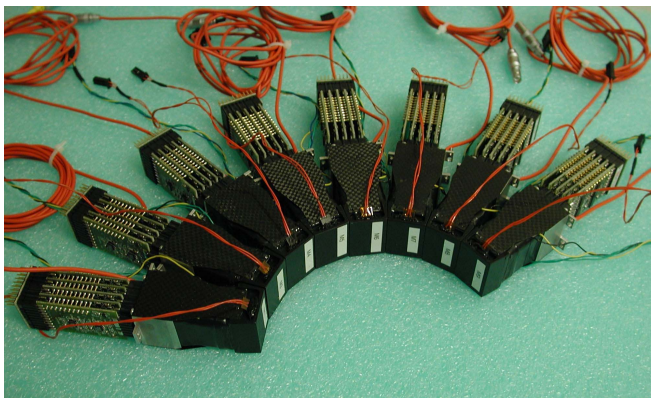

Fig. 2. Picture of 8 LSO/LuYAP phoswich detector heads in final form.

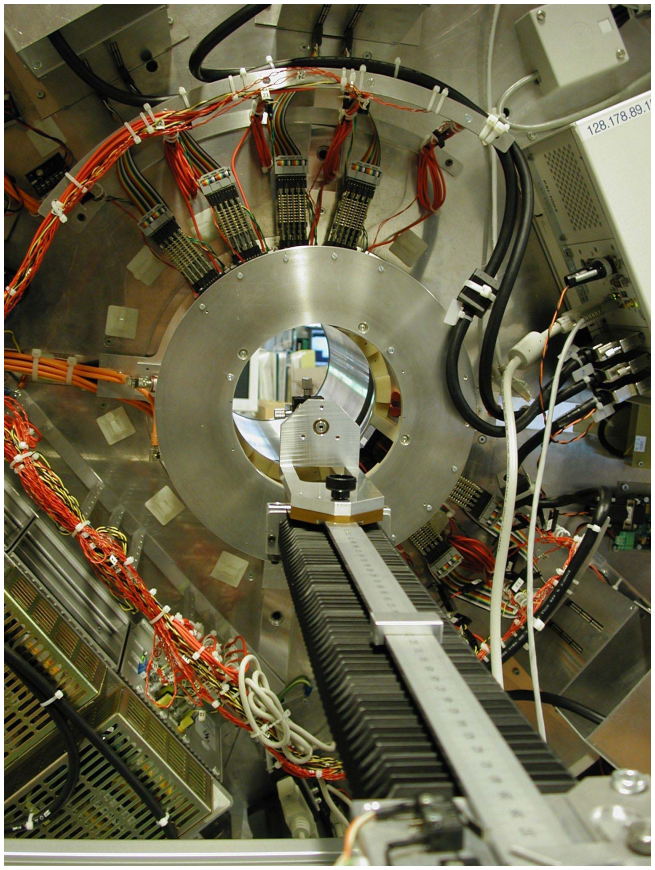

Fig. 3. View of the Lausanne ClearPET camera equipped with 6 detector modules.

### B. Depth of interaction determination

The MCPMT is read out using a free-running sampling electronics at a sampling frequency of 40 MHz. Each pulse readout corresponds to 16 ADC samples $a_i$ ($i$=1,...,16), which cover a time window of 400 ns. The energy is given by the sum of the 16 samples after baseline substraction and DOI is determined from the ratio $r$ of the last sample of the pulse to the sum of the 16 samples, after baseline substraction [9].

$$r = \frac{a_{16} - a_1}{\sum_{i=2}^{16}(a_i - a_1)} \quad (1)$$

While the LSO has a scintillation decay time of 40 ns, the LuYAP has two components in its decay : a fast component with approximately 20 ns decay time and a slow one with approximately 200 ns decay time. Due to the slow component of LuYAP, $r$ is in average larger when the light pulse comes from LuYAP than when it comes from LSO, and hence provides DOI discrimination.

### C. Equalisation of the LSO and LuYAP light collection

The light yield of LuYAP is about one quarter of the LSO light yield. Since the dynamic range of the detector electronics is limited by crosstalk between the MCPMT channels, and in order to optimise the leading-edge trigger threshold that is common to the 64 channels of the MCPMT, it is mandatory to make the LuYAP and LSO light responses as close as possible. Therefore, a thin aluminium layer of 20-35 nm is applied by evaporation on the LSO crystal section facing LuYAP. For each matrix, the thickness of the aluminium layer is determined from the ratio between the measured LSO and LuYAP light yields. This aluminium layer acts as a semi-transparent mirror which slightly increases light collection of LuYAP and absorbs a fraction of the LSO scintillation light. Moreover, the light yields of LSO and LuYAP crystals being temperature dependent [10], a precise matching of the light responses of LSO and LuYAP is obtained by regulating the temperature of the phoswich head between 30 to 60°C. For this, a kapton thermofoil is used to heat the crystal array and maintain the crystals at the appropriate temperature.

### D. Spatial resolution

Figure 3 shows the Lausanne ClearPET demonstrator equipped with 6 detector modules mounted asymetrically so that only two modules are facing each other. The distance between the front face of the pair of detectors mounted along a diameter is 141 mm. Detectors are rotating continuously around the field-of-view (FOV) at an angular speed of 1 rpm. Measurements of the spatial resolution were performed with a $^{22}$Na point source of 3.2 MBq. Acquisition duration for each source position is 60 s.

For each source position, images were reconstructed using the 3D reprojection algorithm [11] implemented in the Software for Tomographic Image Reconstruction (STIR) library [12], [13] with a maximum ring difference of 8 rings. Resolution estimates were derived from Gaussian fits of reconstructed source profiles and compared with Monte Carlo simulations performed using GATE [14], [15]. Monte Carlo data were simulated for a full ring geometry and stored using the same format as for measured data. Positron range and photon acolinearity were not modelled in the simulation. Both measured and simulated data were then processed using exactly the same procedure.

## III. Results and Discussion

### A. Determination of the depth of interaction

Figure 4 shows the distribution of $r$ fitted by a sum of two Gaussians, for one pixel. Assuming that the LSO light pulse distribution follows the Gaussian curve on the left, and the LuYAP one the curve on the right, every pulse with $r$ greater than a DOI discrimination threshold $r_0$ is identified as coming from LuYAP.

Under this assumption, the threshold which minimize the errors of identification were calculated for each pixels of two modules. The mean value of the threshold calculated over all the pixels is equal to $-0.005$ and its standard deviation is equal to 0.001. With a threshold of $-0.005$, the mean correct identification efficiency is better than 98%.

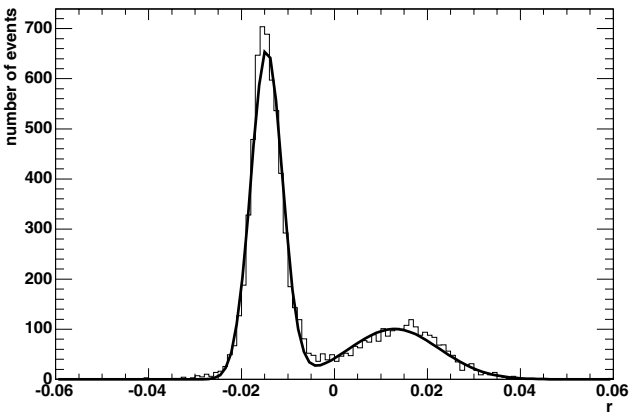


Fig. 4. Distribution of $r$ for one pixel fitted by the sum of two Gaussians.

### B. Equalisation of the LSO and LuYAP light collection

The optical coupling improves the light collection by a factor 2.3 for LuYAP and 1.3 for LSO. The aluminium layer on LSO increases the LuYAP response by a factor 1.09. Figure 5 shows the LSO and LuYAP photopeak position averaged over all the 64 pixels of a module measured as a fonction of temperature. In this case, the LSO and LuYAP responses appear to be similar near 50˚C. LSO and LuYAP have relative temperature coefficients of $-0.71\%/^{\circ}$C and $0.65\%/^{\circ}$C, respectively. Temperature of equalisation is comprised between 37˚C and 54˚C, depending of the thickness of the aluminium deposit with a temperature to thickness dependence of about 5˚C/nm. Once equalised, the ratio between the LSO and LuYAP responses averaged over all the 64 pixels of a phoswich module are comprised between 1 and 1.04.

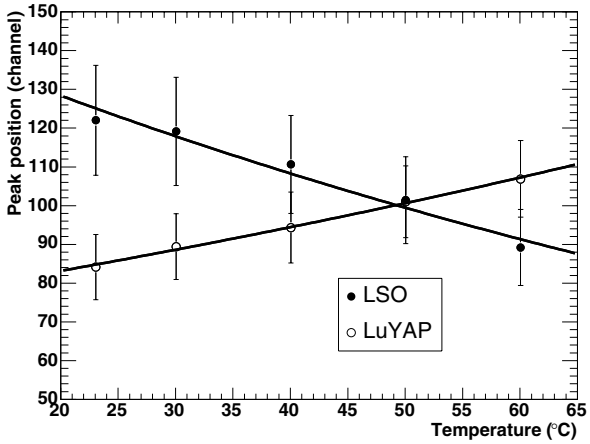


Fig. 5. Average photopeak position with r.m.s. error bars versus temperature.

Figure 6 shows typical LuYAP and LSO energy spectra read out for a MCPMT channel. The ratio between the LSO and LuYAP photopeak amplitudes reflects the photon cross-sections of LSO and LuYAP, with LSO being at the front face of the detector head.

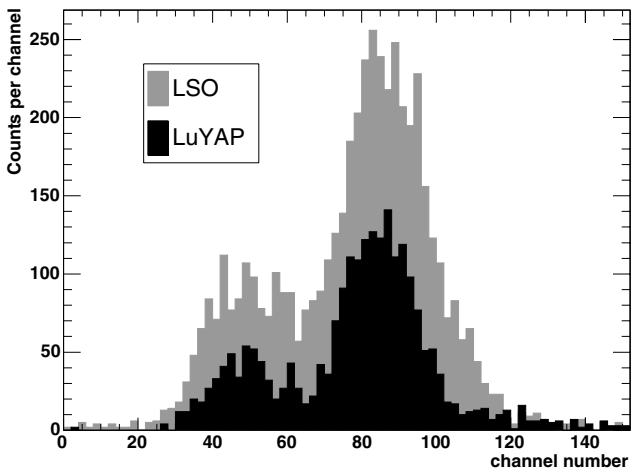


Fig. 6. LuYAP and LSO energy spectra of a $^{68}$Ge source measured with a phoswich head regulated at 48˚C.

### C. Spread of the photopeak position

Figure 7 (left) shows the LSO and LuYAP photopeak positions of the 64 pixels of a phoswich module. The spread of the

photopeak position is mainly due to the non uniformity of the PMT responses, despite the use of a light attenuating mask. The relative standard deviation of the photopeak position averaged over the 8 modules is 11.4% for LSO and 8.0% for LuYAP.

### D. Energy resolution

Figure 7 (right) shows the LSO and LuYAP FWHM energy resolutions of the 64 pixels of a phoswich module. Typical mean FWHM energy resolution within a phoswich module is $(28 \pm 2)\%$ for LSO and $(25 \pm 2)\%$ for LuYAP. LuYAP appears to provide a slightly better energy resolution than LSO when photopeak responses are equal, probably because LuYAP instrinsic energy resolution is better than for LSO [16].

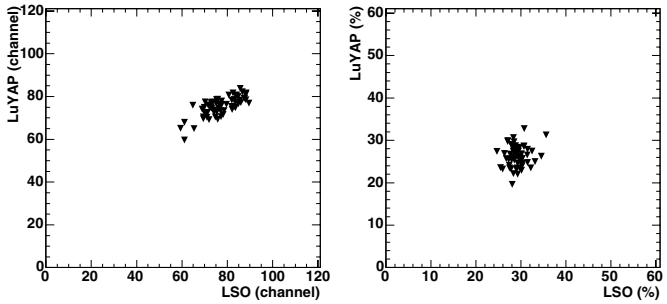


Fig. 7. LSO and LuYAP photopeak positions of the 64 pixels of a phoswich head (left) and FWHM energy resolutions (right).

### E. Spatial resolution

Figure 8 and 9 show the measured and simulated spatial resolutions as a function of the distance between the source and the scanner axis. Results are in excellent agreement for both the radial and tangential resolutions.

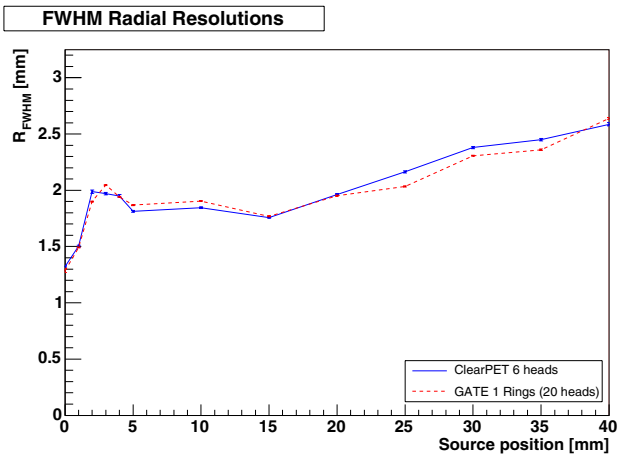


Fig. 8. Measured and simulated radial resolutions.

Figure 10 shows transaxial image slices of a 3.2 MBq $^{22}$Na point source located every 5 mm along a scanner radius up to 4 cm. The 3D sinograms for each source positions are summed without normalisation before reconstruction.

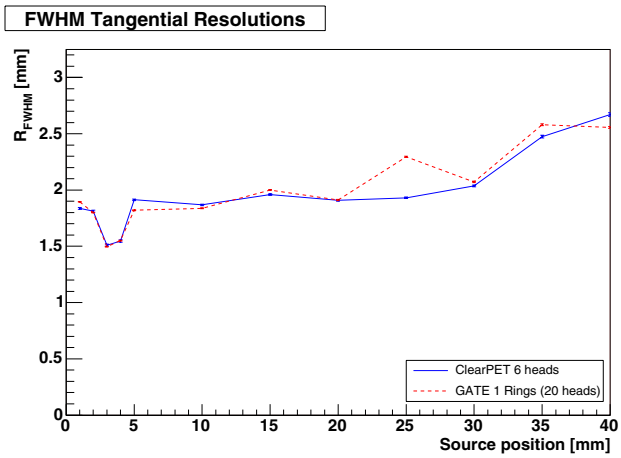


Fig. 9. Measured and simulated tangential resolutions.

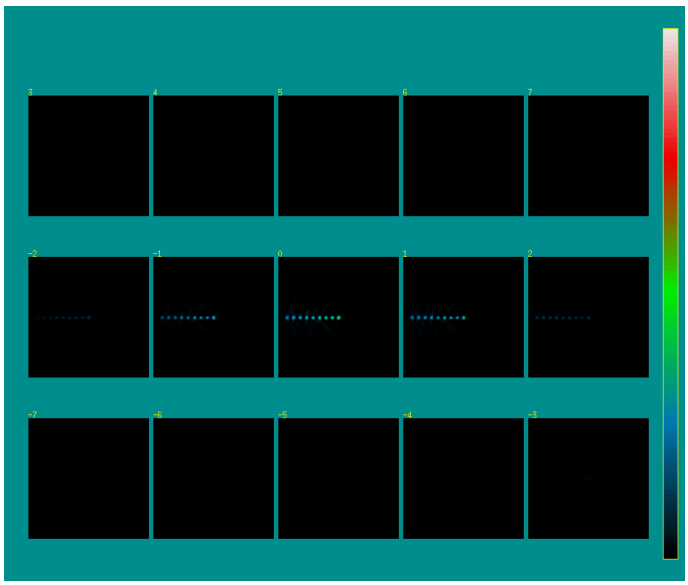

Fig. 10. Transaxial image slices of a $^{22}$Na point source located at 9 different positions every 5 mm from the scanner axis.

## IV. Conclusion

LSO/LuYAP phoswich detector heads have been developed and optimised. Optimisation is obtained through partial attenuation of the LSO scintillation light and appropriate temperature regulation of the phoswich head. The LSO versus LuYAP crystal identification efficiency is better than 98%. The FWHM energy resolution is $(28 \pm 2)\%$ for LSO and $(25 \pm 2)\%$ for LuYAP. The excellent agreement between the measured and simulated spatial resolutions attests for the precision of the positioning of the crystals and for the efficiency of DOI identification performed by the phoswich heads.

## References

[1] E. Auffray *et al.*, "The ClearPET project", *Nucl. Instr. Meth.* A527, pp. 171-174, 2004.

[2] A. Saoudi *et al.*, "Investigation of depth-of-interaction by pulse shape discrimination in multicrystal detectors read out by avalanche photodiodes", *IEEE Trans. Nucl. Sci.*, vol. 46, pp. 462-467, 1999.

[3] M. Schmand *et al.*, "Advantages using pulse shape discrimination to assign the depth of interaction information (DOI) from a multi layer phoswich detector", *IEEE Trans. Nucl. Sci.*, vol. 46, pp. 985-990, 1999.

[4] C.L. Melcher and J.S. Schweitzer, "Cerium-doped lutetium oxyorthosilicate : a fast, efficient new scintillator", *IEEE Trans. Nucl. Sci.*, vol. 39, pp. 502-505, 1992.

[5] J. Chval *et al.*, "Development of new mixed $Lu_x(RE^{3+})_{1-x}AP$ :Ce scintillators ($RE^{3+}$ = $Y^{3+}$ or $Gd^{3+}$) : comparison with other Ce-doped or intrinsic scintilling crystals", *Nucl. Instr. Meth.*, A443, pp. 331-341, 2000.

[6] C. Kuntner *et al.*, "Scintillation properties and mechanism in $Lu_{0.8}Y_{0.2}AlO_3$ :Ce", *Nucl. Instr. Meth.*, A486, pp. 176-180, 2002.

[7] C. Kuntner *et al.*, "Scintillation properties of mixed LuYAP crystals in view of their use in a small animal PET scanner in phoswich configuration", *IEEE Trans. Nucl. Sci.*, vol. 50, pp. 1477-1482, 2003.

[8] D. Christ *et al.*, "Homogenization of the multi-channel PM gain by inserting light attenuating masks", *IEEE Nucl. Sci. Symposium Conference Record 2003*.

[9] M. Streun *et al.*, "Pulse Shape Discrimination of LSO and LuYAP Scintillators for Depth of Interaction Detection in PET", *IEEE Trans. Nucl. Sci.*, vol. 50, pp. 344-347, 2003.

[10] S. Weber *et al.*, "Comparison of LuYAP, LSO, and BGO as Scintillators for High Resolution PET Detectors", *IEEE Trans. Nucl. Sci.*, vol. 50, pp. 1370-1372, 2003.

[11] P.E. Kinahan and J.G. Rogers, "Analytic 3D image recontruction using all detected events", *IEEE Trans. Nucl. Sci.*, vol. 36, pp. 964-968, 1989.

[12] C. Labbé *et al.*, "An object-oriented library incorporating efficient projection/backprojection operators for volume reconstruction in 3D PET", in *Conf. Rec. of the Int. Meeting on Fully Three-Dimensional Imag. Rec. in Radiol. and Nucl. Med.*, Egmond aan Zee, edited by F. Beekman, M. Defrise, and M. Viergever, Utrecht, NL, pp. 137-140, 1999.

[13] *http ://stir.hammersmithimanet.com/* [Online]

[14] G. Santin *et al.*, "GATE : a Geant4-Based Simulation Platform for PET and SPECT Integrating Movement and Time Management", *IEEE Trans. Nucl. Sci.*, vol. 50, pp. 1516-1521, 2003.

[15] S. Jan *et al.*, "GATE : a simulation toolkit for PET and SPECT", *Phys. Med. Biol.*, vol. 49, pp. 4543-4561, 2004.

[16] C. Kuntner *et al.*, "Intrinsic energy resolution and light output of the $Lu_{0.7}Y_{0.3}AlO_3$ :Ce scintillator", *Nucl. Instr. Meth.*, A493, pp. 131-136, 2002.